Journal of Ocean Engineering and Marine Energy (2021) 7:421–438
https://doi.org/10.1007/s40722-021-00211-0

RESEARCH ARTICLE

Hydrodynamic performance of planing craft with interceptor-flap hybrid combination

J. Suneela[1] · P. Krishnankutty[1] · V. Anantha Subramanian[1]

Received: 1 March 2021 / Accepted: 15 July 2021 / Published online: 26 July 2021

Abstract
Different innovative ideas on simple stern fixtures such as stern wedges, flaps, interceptors have evolved over the past few years to improve the hydrodynamic performance of high-speed vessels, including planing crafts. This paper examines the hydrodynamic performance of a planing craft fitted with an interceptor alone and also an interceptor-flap combination at its stern, and the results are compared with the case where the craft uses the interceptor alone. An interceptor-flap combination is the one where an interceptor extends vertically downward at the transom with a flap attached to its end. Different angular orientations of the flap attached to interceptor bottom end and project towards aft are considered in the present study. The effectiveness of the integrated interceptor-flap system on the hydrodynamic performance of the vessel is influenced by the angular orientation of flap to the interceptor. Experiments were carried out on a planing hull with and without interceptor in the towing tank, Department of Ocean Engineering, Indian Institute of Technology Madras. Computational fluid dynamics (CFD) simulations are performed for the planing hull fitted with an integrated interceptor and flap. The investigations look into the aspects of vessel resistance, trim and bottom pressure distribution while it operates in calm water condition and at different speeds. The results show that trim and resistance of the vessel reduce with the use of integrated interceptor-flap at the stern with the flap angle at about 4° to the horizontal and they are less compared with a case where the only interceptor is used.

Keywords Planing craft · Interceptor · Stern flap · Resistance · Trim

List of symbols

B	Breadth of hull
CFD	Computational fluid dynamics
C_T	Total resistance coefficient
C_P	Pressure resistance coefficient
C_G	Correction factor
D	Experimental data
DFBI	Dynamic fluid body interaction
DOF	Degree of freedom
E	Comparison error
Fr_B	Beam Froude number
h	Boundary layer thickness
ITTC	International Towing Tank Conference
k	Turbulent kinetic energy
L	Length of hull
L_K	Wetted keel length
LCG	Longitudinal center of gravity
P	Average pressure field
P_G	Order of accuracy
R_t	Resistance of vessel
RANSE	Reynolds averaged Navier–Stokes equations
R_G	Grid convergence ratio
r_k	Refinement ratio
R_k	Convergence ratio
Re	Reynolds number
SIMPLE	Semi implicit pressure linked equations
S_W	Wetted surface
S_M	Momentum source vector
S	Simulation results
T_{RE}	Reynolds tensor stress
U_{SN}	Numerical simulation uncertainty
U_I	Inner iterations uncertainty
U_T	Time-step uncertainty
U_P	Statistical error uncertainty
U_V	Validation uncertainty
U_D	Experimental uncertainty
U_G	Grid uncertainty

✉ V. Anantha Subramanian
suneelajangam4@gmail.com

1 Department of Ocean Engineering, IIT Madras, Chennai 600036, India

V	Speed of vessel
VOF	Volume of fluid
β	Deadrise angle
Δ	Displacement of vessel
Δt	Time step
g	Acceleration due to gravity
μ	Dynamic viscosity
μ_t	Turbulent viscosity
ρ	Density of fluid
τ	Running trim

1 Introduction

Planing hulls are high-speed crafts in which the hydrodynamic forces play a more predominant role than the hydrostatic forces on its performance. The resistance of a high-speed vessel is important with regard to its power requirement and fuel consumption. Knowledge of basic hydrodynamic characteristics of planing surfaces is necessary to understand its performance. Hence, due attention is given by Savitsky (1964) on the planing hulls by considering appropriate relations between wetted area, lift, drag, deadrise angle, trim angle and forward speed. His initial investigations looked into essential hydrodynamic characteristics of prismatic planing hull form and formulated simple approaches to predict the vessel power requirements, running trim, draft, and porpoising stability. As resistance is also important in high-speed hulls various methods are used to reduce resistance which helps in the reduction of fuel consumption. Various techniques are used by Faltinsen (2005) to find effective ways in reducing resistance. The frictional and pressure resistance are the main components which directly influence the hydrodynamic performance of the vessel. The reduction in pressure drag is achieved mainly by improving the hull form. Hoekstra (1999) and Li et al. (2002) reported that wave making resistance is also one of the component that is to be considered in high-speed hulls. Frictional resistance is dominant in the total resistance of vessels. Nowadays detailed prediction of flow around the hull is easily found by using viscous flow computations (Raven and Brummelen 1999). To analyse the frictional resistance which is a combination of viscous and wave resistance CFD techniques are used by applying the turbulence model as reported by Insen et al. (1999). Millward (1976) moved a step ahead and carried out tests on the DTMB Series 62 hulls with different wedges at the bottom of planing hulls and showed that the wedge may positively help to reduce the resistance, control the trim, and avoid the proposing phenomenon. It was concluded that the wedge length and wedge angle have to be a function of displacement, LCG position and speed. The stern wedge is located beneath the transom at an angle relative to the buttock as shown in Fig. 1a.

Numerical study on the resistance performance with transom wedge for fast-ferry was carried out by Hung and Kim (2007) and observed that the transom wedge plays a vital role in pressure recovery resulting in improved resistance performance. Further, the research was moved to experimenting with stern flap. It is an extension of the hull bottom surface, which extends aft of the transom as shown in Fig. 1b.On similar lines experimental study on powering improvements for DDG 51 flight class ships was carried out by Karafiath et al. (1999). It was observed that transom wedge and flap play an important role in the reduction of fuel consumption. Jose et al. (2012) investigated the hydrodynamic behaviour of a small high-speed displacement craft and the resistance of the planing craft using the classical work of Savitsky by attaching stern flaps. The improvement of the hydrodynamic behaviour of the crafts with the use of stern flap was found only up to a certain velocity range. Anantha Subramanian et al. (2007) computed the tunneled planing hull resistance and trim angle using a numerical method and found a reduction of resistance and trim on the planing hull with a tunnel. Stern wedges, flaps and trim tabs are being used in many small high-speed vessels such as workboats, patrol crafts, and pleasure crafts.

Stern interceptor (see Fig. 2a) is another appendage like flaps, wedges or trim tabs being used to control trim in high-speed vessel. The interceptor application in high-speed craft and the idea of interceptor design was originated from transom flaps. An Interceptor is a thin plate fitted at the transom of a craft, projecting slightly below its bottom uniformly. Figure 3 shows the interceptor attached with flap (S is span and C is chord) at the transom bottom of the planing craft model used in the present study. The interceptor extends vertically downward at the transom, as shown in Fig. 2a and

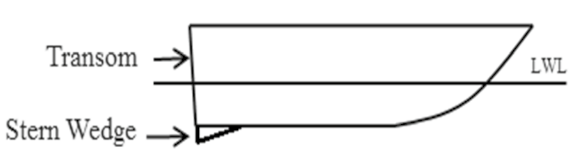

(a) Hull with a stern wedge

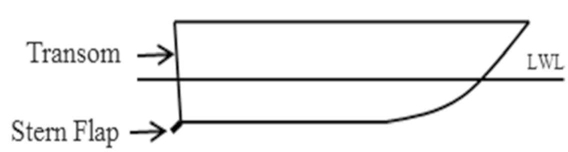

(b) Hull with stern flap

Fig. 1 Schematic diagram of **a** stern wedge and **b** stern flap fitted to a planing hull

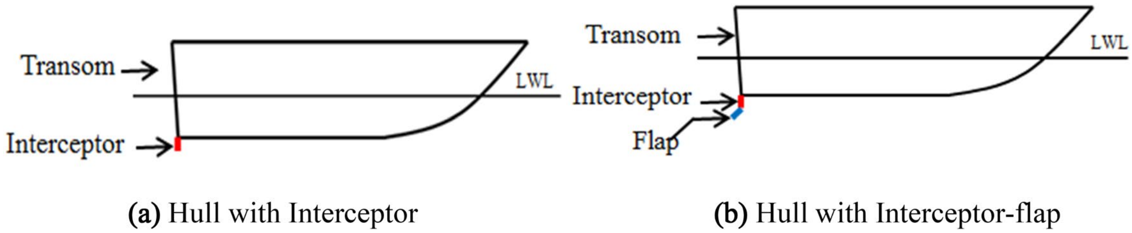

Fig. 2 Schematic diagram of **a** stern interceptor, **b** integrated interceptor-flap

Fig. 3 CAD model of planing hull

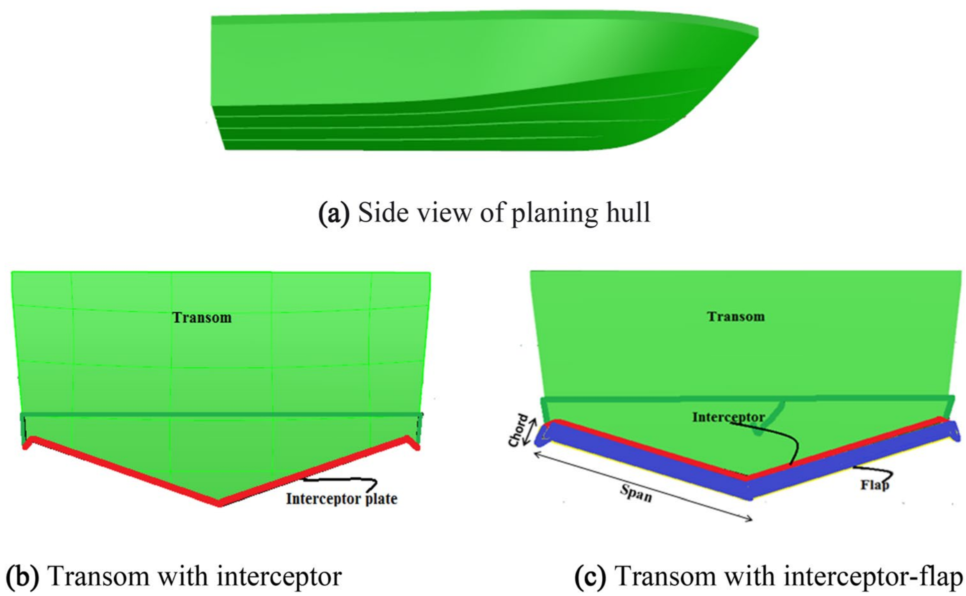

the interceptor-flap combination is shown in Fig. 2b. Brizzolara (2003) and Molini and Brizzolara (2005) carried out numerical studies on vessels fitted with interceptors. They presented the pressure and velocity distributions around the transom and reported that lift produced by interceptors is proportional to blade height and square of inflow velocity. Villa and Brizzolara (2009) studied the comparative performance of prismatic planing hulls fitted with stern flaps and interceptors.

Deng et al (2011) observed that the use of an interceptor with appropriate height reduces ship resistance at different speeds. Ghassemi et al. (2011) numerically studied and presented the hydrodynamic forces caused by interceptor on a planing hull resulting in the vessel trim reduction by aft. Srikanth Syamsundar and Datla (2008) used prismatic planing hull with interceptors to study the effect of trim and drag on planing hull.

De Luca and Pensa (2011) investigated experimentally the hydrodynamic performance of three prismatic planing hulls with deadrise angles of 10°, 20° and 30° for a beam Froude number range of 1.3–2.8 and with different depths of interceptor. Mansoori and Fernandes (2015) carried out both numerical and experimental studies on 2D flat plates fitted with interceptors to determine their effects on the hydrodynamic pressure and forces acting on the plate. Mansoori et al. (2017) conducted numerical and experimental studies to find the effect of interceptor height and deadrise angle on planing hull performance. They have also looked into the boundary layer thickness at the stern on the interceptor effectiveness in improving the hull performance. Mansoori and Fernandes (2017a, b) carried out numerical study on planing boat with 10° dearise angle fitted with interceptor and trim tab and found reduction in resistance and trim. The experimental investigations of Avci and Barlas (2018) on high-speed crafts with interceptors of different positions at stern found that performance is better when interceptor is placed at the bottom. Suneela et al. (2020) numerical study on planing craft model observed that the height of interceptor plays an important role on the performance of vessel.

Day and Cooper (2011) studied the effectiveness of interceptors and compared them with an aerodynamic flap device in a sailing yacht and concluded that there is 10–18% fuel saving with reduced sinkage and trim. Tsai et al (2004) experimentally worked on two patrol boats of different lengths with and without interceptors and flap combination. Suneela et al. (2018) carried out a numerical study on interceptor-flap for a planing hull. The results proved that well-designed trim mechanism can reduce both the running trim and the resistance of the planing hull. John et al (2011) studied experimentally the effect of flaps, wedges and interceptor on different types of vessels like displacement vessel, catamaran, and a planing hull and found that these fixtures at the stern improved the performance of the planing hull compared to the displacement vessel. Salas and Gonzalo (2013) carried out CFD study on a displacement hull fitted with stern flaps and interceptor and also on a semi-planing hull having spray rail and found that the effects of flaps and interceptors are more on the semi-planing hull where the resistance got reduced by 10%. Experimental investigations were carried out by Karimi et al. (2013) on the performance of stern interceptors and flaps on high-speed planing hull and displacement type catamaran and found that the reduction of resistance in planing hull is more compared to the catamaran. Song et al (2018) conducted SPIV and numerical studies on waterjet-propelled ship with interceptor and observed that interceptor's retarding effect to be the main factor driving changes in inlet velocity distribution.

The application of integrated interceptor-flap (see Fig. 2b) in high-speed planing crafts is compared to other stern fixtures such as interceptor, flap, and wedge. Higher flow kinematics at a planing vessel aft region results in a pressure reduction in this region, resulting in excessive trim of the vessel by aft and consequent augmentation in the vessel resistance and power requirement. It has been generally observed from the studies that a reduction in trim by aft reduces the planing vessel resistance, particularly when it operates at high speed. The trim reduction can be achieved by increasing the hydrodynamic pressure in the aft area. The different stern fixtures discussed above help in the pressure enhancement in the vessel aft region and consequent reduction in trim and vessel resistance. The integrated interceptor-flap also work with the same principle where the flow gets retarded at the aft region due to its presence, and thus the hydrodynamic pressure builds up resulting in a reduction of trim by aft. Advancement in computational facilities and CFD techniques have improved the accuracy in capturing the flow characteristics around more complicated flow situations like the one around high-speed vessels with different appendages. The integrated interceptor-flap (see Fig. 3) application in high-speed vessels being a relatively new concept on 20° deadrise hulls, studies and the literature on its parametric variations and effects are scanty.

This paper presents the studies carried out to find the effect of interceptor and integrated interceptor-flap fitted to the transom of the planing hull with 20° deadrise angle. Both numerical and experimental studies are carried out with the vessel for the cases with and without interceptors, where both heave and pitch degrees of freedom for the vessel were allowed. Numerical studies for both cases were performed using commercial CFD software (Star CCM), and the experiments were conducted in the towing tank facility at the Department of Ocean Engineering in IIT Madras. These results were compared and validated against each other. The numerical studies were further continued for the case where the planing vessel is fitted with interceptor-flap at different speeds in planing regime. Section 3 presents the methodology used to carry out numerical simulations in the RANS-based software and Sect. 4 presents the experimental setup used in the present study. Section 5 presents and discusses the results, followed by Sect. 6 on the summary of the work and conclusions drawn.

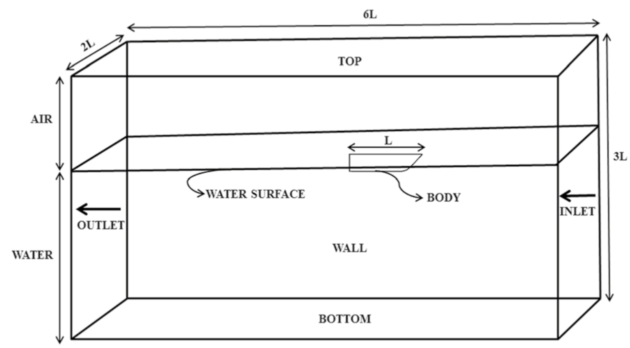

Fig. 4 Computational domain with boundary conditions

Table 1 Principal particulars of the planing hull

Particulars	Prototype	Model (scale 1:25)
Length, L [m]	20.5	0.82
Breadth, B [m]	5.30	0.212
Draft, T [m]	1.062	0.043
Displacement, Δ [kg]	46,000	2.94
LCG from the transom, [m]	6.50	0.26
Interceptor height, [mm]	25.0	1.0
Design speed, V	25knots	2.57 m/s
Deadrise angle, β [°]	20 20	

2 Vessel particulars

The planing hull vessel CAD model used for the present studies is shown in Fig. 4, and its particulars are given in Table 1. The vessel has a deadrise angle of 20°. The interceptor height is 25 mm in the prototype, which is equal to 1.0 mm in the model scale of 1:25. The vessel design speed is 25.0 knots, leading to a corresponding model speed of 2.57 m/s.

3 Numerical study

Computational fluid dynamics has become a strong tool for analysing complex flow problems such as the one considered here. A commercial RANSE based code (Star CCM) is used here to numerically study the flow variations around the planing vessel, where the dynamic changes like trim, sinkage and bottom pressures and hydrodynamic forces are estimated. The hull with and without interceptor and with the integrated interceptor-flap fitted at the transom of the planing hull are the different cases which are simulated using the software.

3.1 Governing equations

The equations which govern the fluid flow are the continuity and Navier–Stokes equations. More complex flows can be handled numerically with CFD techniques such as the finite volume method (FVM) without additional approximations. The ship hydrodynamic flows are, however, turbulent. So, these flows are carried out with procedures based on RANS equations. These equations can be expressed, in the hydrodynamic applications, as an incompressible flow as

$$\Delta \cdot V = 0, \tag{1}$$

$$\rho \frac{\partial V}{\partial t} = -\nabla P + \mu \Delta V + \nabla \cdot T_{\mathrm{RE}} + S_{\mathrm{M}}, \tag{2}$$

where V is the Reynolds averaged velocity vector, P is the average pressure field, μ is dynamic viscosity, T_{RE} is Reynolds tensor stress and S_{M} is momentum source vector.

The component of T_{RE} is computed using the selected turbulence model, in agreement with Boussinesq hypothesis.

$$\tau_{ij}^{Re} = \mu_t \left({}^{\partial V_i}_{\partial x_j} + {}_{\partial x_i}{}^{\partial V_j} \right) - \frac{2}{3} \rho k \delta_{ij}, \tag{3}$$

where μ_{t} is turbulent viscosity, k is turbulent kinetic energy. There are many turbulence models in RANS method for the hydrodynamic problem, but widely used turbulence models are those two-equation models, such as k–ω SST and the Realizable k–ε. The physical model is discretized based on FVM using RANS based solver.

3.2 Modelling

The main particulars of the vessel used for the present study are shown in Table 1. The CAD model used for the numerical study is shown in Fig. 3. Figure 3a represents the profile view of the CAD model, Fig. 3b shows the interceptor plate fitted to the transom protruding down the bottom by 1 mm (equivalent to 25 mm in prototype). Figure 3c shows the transom with interceptor-flap, with the flap chord length taken as 2.5% of vessel length and its span across the transom at the bottom. The flap is fitted at the lower end of the interceptor, and its angular orientations are taken as 0°, 4° and 8° down with respect to the horizontal.

3.3 Computational domain

The computational domain (see Fig. 4) is one vessel length (L) in the front of the bow to the inlet boundary, 4L behind the vessel transom to the outlet boundary, 2L below the keel down to the bottom boundary and L from the hull side to the wall boundary. The computational domain used here is consistent with the one recommended by ITTC (7.5-03-02-03) (2011).

3.4 Boundary conditions

The boundary conditions used in the simulation are given in Table 2.

The inlet, bottom, side and top boundaries are prescribed with velocity inlet, outlet boundary as pressure outlet which is placed far enough to ensure the flow is fully developed so that no reflections occur in the direction of flow. Body surface is taken with a no-slip boundary condition. Exploiting the problem symmetry, only half body and domain in the longitudinal plane are considered for the CFD analysis, to reduce the computational effort. The normal velocity and normal gradients of all variables are zero at the symmetry plane.

3.5 Grid generation

The mesh generated here uses the overset option, in which there are two different regions of meshing surrounding the body, one is overset mesh and the other is background mesh. In the background mesh, the meshes are static and in the overset mesh, the mesh moves along with the hull. Table 3 shows the grid independence study carried out here for the proper selection of grid size. Convergence of the simulations are considered by ensuring that we have a valid solution where residual RMS error values are reduced to

Table 2 Boundary conditions

Surface	Boundary condition
Inlet	Velocity inlet
Bottom	Velocity inlet
Side	Velocity inlet
Top	Velocity inlet
Outlet	Pressure outlet
Symmetry	Symmetry plane
Body	Wall (no slip)

Table 3 A sample of grid independence study at $Fr_B = 1.78$

Grid	Cells	R_t/disp.
A	1,342,099	1.45
B	1,925,202	1.51
C	2,806,668	1.53
Experiment	–	1.49

an acceptable value of 10^{-4} or 10^{-5} and monitor points for values of main output like drag force and pressure. We have to make sure that these have converged to a steady value. From the grid independence study, Grid B is selected for the numerical simulation. In certain regions like the free surface of the computational domain, it is necessary to reduce the cell size to capture the flow. The STAR-CCM + FVM solver uses the volume of fluid (VOF) method which simulates the equivalent properties of immiscible fluids and captures the interface between the phases. The use of the two-phase VOF model solves a single set of conservation equations for mass, momentum and energy for an equivalent fluid phase. This model assumes that all the phases in a control volume (air or water) share the same flow field properties. Therefore, no boundary condition is required at the interface. The model calculates fluid properties such as density and viscosity are based on the corresponding properties of the constituent phases and their volume fractions. The volume fraction of each phase of particles in the flow domain is solved from a particle continuity equation, which is an Eulerian approach. The cell size around the hull is made small and 4–5 cells are given across the spray rails to analyse the flow field.

Prism layers are generated adjacent to the hull to capture the boundary layer flow accurately and ten prism layers are considered in this study. The wall $y+$ values are taken between 30 and 130 over the hull. The time-step (Δt) should be small enough to resolve the motion of the free surface. The time-step used in the simulations is a function of hull speed (V) and dynamic waterline length (l) and the same is determined using Eq. (4), as given by ITTC (7.5-03-02-03) (2011).

$$\Delta t = 0.01 \sim 0.005\frac{l}{V}, \tag{4}$$

3.6 Solver settings

The solver settings used in the simulation are given in Table 4. Volume of fluid (VOF) method which is a free surface modelling technique is used for tracking and locating the free surface. The dynamic fluid body interaction (DFBI) is used to simulate the motion of the body according to the forces acting on it induced by the flow.

Table 4 Solver parameters

Parameter	Settings
Solver	3D, unsteady, implicit
Turbulence model	Realizable k–ε
Pressure–velocity coupling	SIMPLE
Multiphase model	Volume of fluid (VOF)
Wall treatment	Two layers all wall $y+$ treatment
Time discretization	First order upwind
Number of inner iterations	10
Overset interpolation scheme	Linear

The turbulence model used is realizable k–ε, where k is the turbulent kinetic energy and ε, is the rate of dissipation of turbulent kinetic energy. De Luca et al. (2016) identified the accuracy of numerical investigations with experimental studies. The model simulates the mean flow characteristics for turbulent flow conditions. The scheme used for the interface between background mesh and overset mesh is a linear interpolation. The interpolation function builds the coefficient matrix of the algebraic equation system (Star CCM + user guide 2014). The solution computes the flow parameters for all active cells in the overlap region. The ship was allowed to move with two degrees of freedom to account for sinkage and trim.

4 Grid verification study

Verification is defined as a process for assessing simulation numerical uncertainty U_{SN} and estimating the simulation numerical error (δ_{SN}) itself and the uncertainty in that error estimate. Verification analysis is performed for overset mesh method used here in this study. The verification is carried out for the response variables namely, total resistance coefficient (C_T), pressure resistance coefficient (C_F), wetted surface area (S_W) and running trim (τ) at a design speed of 25 knots that corresponds to 2.57 m/s for the model. The numerical uncertainty U_{SN} is composed of iterative percentage of the solution with 10 inner iterations U_I, time-step uncertainity U_T, grid uncertainties U_G and the uncertainity due to statistical errors U_P.

The verification study of the CFD simulations is performed based on the methodology prescribed in Stern et al. (1997) and Stern et al. (2001). Verification is defined as a process for assessing simulation numerical uncertainty, $\boldsymbol{U_{SN}}$ RMS addition. Based on and Stern et al. (2001) the combined numerical uncertainty is estimated by RMS addition given by,

$$U_{SN} = \sqrt{U_I^2 + U_G^2 + U_T^2 + U_P^2}. \tag{5}$$

The verification process for many common input parameters (e.g. grid spacing, time-step and artificial dissipation) are conducted using the multiple solutions method. To do this it is necessary to use a minimum of three solutions ($m=3$) which have been uniformly refined with an increment Δx_k that defines a constant refinement ratio r_k

$$r_k = \frac{\Delta x_{km}}{\Delta x_{km-1}}. \tag{6}$$

The data obtained from grid dependency analysis is given in Table 14; the analysis uses the correction factor method prescribed in Stern 2001. It is established that the condition for monotonic convergence is achieved since for all the response variables considered, the grid convergence ratio (R_G) is less than one.

ITTC Guidelines (2008) recommend for the industrial application refinement ratio (r_k) between $\sqrt{2}$ and 2.

Next a convergence ratio R_k was defined to give information about convergence/divergence of a solution.

This is achieved by considering the solution changes ε_{ijk} for the input parameter k between three solutions ranging from fine S_{k1} to medium S_{k2} and coarse S_{k3}, to determine R_k.

$$\varepsilon_{21k} = S_{k2} - S_{k1}$$

$$\varepsilon_{32k} = S_{k3} - S_{k2}$$

$$R_k = \frac{\varepsilon_{21k}}{\varepsilon_{32k}}. \tag{7}$$

According to the ITTC Guidelines (2008) and the extended versions reported in some works, e.g., Stern et al (2001), four different cases of R_k may occur:

1. Monotonic convergence: $0<R_k<1$;
2. Oscillatory convergence: $R_k<0$, $|R_k|<1$;
3. Monotonic divergence: $R_k>1$;
4. Oscillatory divergence: $R_k<0$, $|R_k|>1$.

In case 1 the generalized Richardson extrapolation (RE) is used to assess the uncertainty U_V or error estimate E are shown in Appendix A.

5 Experiments for validation

5.1 Resistance test setup and procedure

The model selected for the experimental tank test investigations is shown in Fig. 5. In the current study, all the experimental tests are performed in the towing tank at the Department of Ocean Engineering, IIT Madras. The towing tank has dimensions of 85 m length, 3.2 m breadth, and 2.5 m depth. The carriage can achieve a maximum velocity of 4 m/s. The experimental methodology followed for the planing craft resistance tests is in accordance with ITTC Procedures (7.5-02-05-01) (2002) for high-speed marine vehicles resistance test, which is based on the 1978 prediction method. The model was fabricated on a scale 1:25 in rapid prototyping using acrylonitrile butadiene styrene (ABS) material. The pivot set-up was provided with a slot arrangement to slide and fix it at any point along the length of the vessel.

The 1:25 scale for the model was considered based on the limitation of the towing carriage speed. The model was ballasted to the loaded condition of the vessel. The model towing tests were conducted in the speed range of 1.44–3.6 m/s.

The design speed of 2.57 m/s corresponds to a beam Froude number of 1.78 at which the vessel planes. The model with all fittings required for the resistance test was weighed before deploying it into the towing tank water. The ballast weights are added inside the hull to achieve the required trim condition, with no heel and ensuring that the waterline of the floating model matches with the corresponding draft line drawn on the hull. The tow point of the model was attached at the longitudinal centre of gravity (LCG). The model was fixed to the specially designed and fabricated support frame such that it is free to take its natural trim and

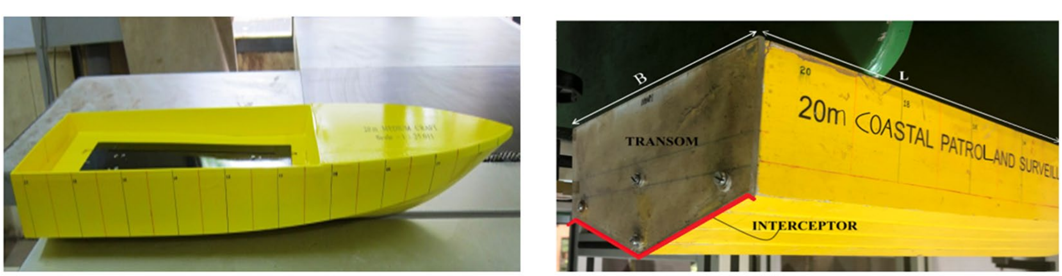

(a) Bare hull model **(b)** Interceptor at the transom

Fig. 5 Model with and without interceptor heave attitude while the carriage tows the model along the centreline without any drift or sway. The model has an initial trim of 1.5°. According to ITTC (7.5-02-05-01) (2002) recommended procedures and guidelines testing and extrapolation methods for High-Speed Marine Vehicles of Resistance Test specified that for models solely at higher Reynolds numbers the turbulence stimulation might be omitted.

The test set-up consists of a precision linear guide system for free sinkage and emergence of the model, a pivot mechanism with block bearings for pitching of the model, a load cell for resistance measurement and counterweight connected to the guide rod, through a pulley to balance the excess weight of the components as shown in Fig. 6. The model tests were performed for the cases with and without interceptor. The interceptor was positioned at the transom with 1.0 mm below the bottom.

5.2 Resistance measurement

The resistance of the towed model was measured using a beam-type load cell. The instrument is connected to HBM PMX; a PC-based electronic measurement system that houses all the components for transducer excitation, amplification and signal conditioning, digitisation, and interfacing with the computer of up to eight transducers. The PMX is configured for the experiments using Catman® software, which manages the settings and calibration data of the measuring instruments. The load cell was calibrated for the measurement range, and the calibration constant is keyed into Catman. During the experiment, the signal data from the load cell pass through PMX and is processed by Catman to display the measured force plots in real-time on the computer by considering the zero corrections, calibrations data, and 50 Hz sampling rate as per the settings. Test runs are performed for various speeds of the model covering the prototype speed range. At the steady speed of the carriage, the load cell readings measuring the model resistance are recorded. Sufficient waiting time was provided between consecutive runs for the free surface disturbances to die out. The recorded data of the measured force for each run is processed to obtain the average tow force value by selecting the data window for the constant speed duration from the time series plot corresponding to the particular speed.

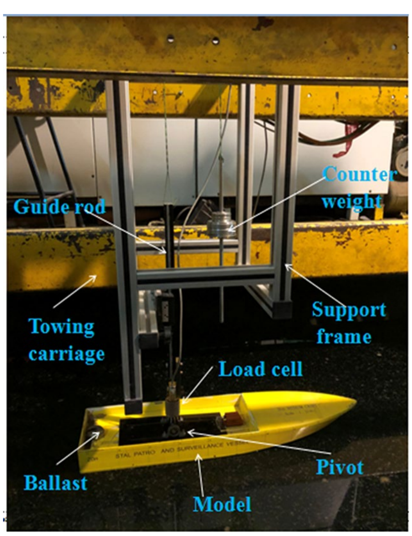

Fig. 6 Resistance test set-up of the model at zero speed

6 Results and discussion

6.1 Resistance and trim (experimental)

A planing vessel model was tested with and without an interceptor at the transom for different speeds. During planing, the weight of the vessel is mainly supported by hydrodynamic pressure, and the vessel usually will have a reduced trim by aft. Based on the experimental results, it is observed that the resistance and trim of the model reduce when an interceptor is used. Figure 7a shows the resistance plot for the hull with and without interceptor. Figure 7b shows the trim variation for the hull with and without interceptor for different beam Froude numbers. The beam Froude number is given by $Fr_B = V/\sqrt{gB}$, where V is the speed of craft, g is the acceleration due to gravity and B is breadth of craft. The trim reduction is more at high speeds when the hull is fitted with interceptor, where the trim reduction increased from 4.23° and 3.4° at beam Froude number 1.57–2.28.

Figure 7 and Table 5 shows the experimental resistance and trim values for the model in the planing regime with and without interceptor. The results show that there is up to 5–15% reduction in hull resistance with the use of 1 mm interceptor (which is equal to 25 mm in prototype) when compared to the hull without an interceptor in the planing regime. The resistance of the hull with and without the interceptor increase with an increase in speed but a reduction of resistance is observed when the hull is fitted with the interceptor. The outcome displays up to 32–45% decrease in trim with interceptor when compared to the hull without interceptor at planing speeds. Experimental results show that there is up to 11% reduction in drag and 37% in trim with the use of interceptor at a model speed of 2.57 m/s ($Fr_B = 1.78$) when compared to the hull without interceptor.

Figure 8 shows the trim variations of the model while it operates at $Fr_B = 1.78$. The trim measured at $Fr_B = 1.78°$ is 6.65° with a resistance of 4.38 N for the hull without interceptor and those for the case with interceptor (Fig. 8) are 4.75° and 4.17 N, respectively. The experimental results show that the trim of the hull with interceptor is less

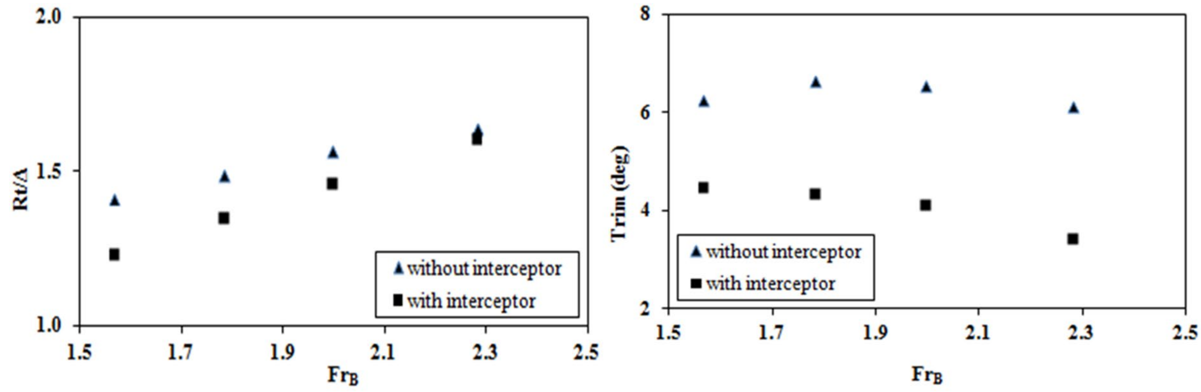

(a) Resistance (b) Trim

Fig. 7 Comparison plot of hull **a** resistance and **b** trim with and without interceptor at different speeds in planing regime (experimental)

Table 5 Resistance and trim values for bare hull and interceptor

Froude number	R_t/Δ (N/kg) (Bare hull)	R_t/Δ (N/kg) (Interceptor)	Trim (°) (Bare hull)	Trim (°) (Interceptor)
1.57	1.41	1.23	6.26	4.48
1.78	1.49	1.35	6.65	4.32
2.0	1.57	1.47	6.58	4.10
2.28	1.64	1.61	6.13	3.41

compared to the hull without interceptor. The trim reduction is due to the pressure created at the transom due to interceptor.

The hull model trim position with and without interceptor, for the $Fr_B = 1.78$, are shown in Fig. 9 for the case where a 2 mm height interceptor is used. Trim is more for the vessel model without interceptor. The trim angle measured is 6.65° without interceptor and the corresponding resistance

(a) Without interceptor **(b)** With 1mm interceptor

Fig. 8 Model trim position (Expt) at $V_m = 2.57$ m/s ($Fr_B = 1.78$)

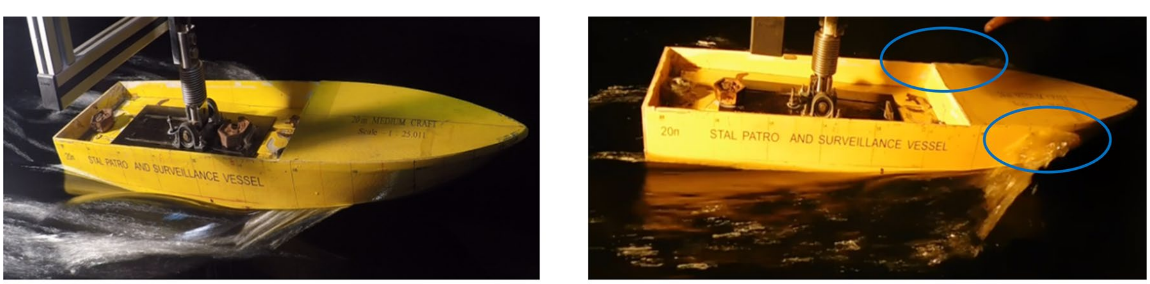

(a) Without interceptor (b) With 2 mm interceptor

Fig. 9 Model trim position (Expt) at $V_m = 2.57$ m/s ($Fr_B = 1.78$)

is 4.38 N. The trim angle for the hull with 1 mm interceptor is 3.25° with a resistance of 3.98 N at $Fr_B = 1.78$. Figure 9b shows the hull with a 2 mm interceptor at the same speed ($Fr_B = 1.78$). The trim angle for the hull with 2 mm interceptor is 2.8° with a resistance of 4.16 N. It is observed that the model with 2 mm interceptor height creates a bow down moment resulting in negative (bow) trim. Figure 9b shows the bow wave is changed with keel length. With the intense pressure created at the transom due to 2 mm interceptor there is negative trim on the vessel and further due to an increase in keel wetted length the resistance on the vessel is increasing where the loss of energy is visible. The study shows that a choice of the right height for the interceptor gives a favourable trim and reduction in vessel resistance. Based on the present study, a height of 1 mm for the interceptor is preferred for the vessel than 2 mm height. No studies are carried out here with intermediate heights for the interceptor to fine tune the interceptor hydrodynamic advantage experimentally, but numerical studies were performed for different heights (Suneela et al. 2020).

6.2 Comparison of CFD with experimental

The planing hull model is simulated using the present CFD model to check the validity of the numerical setup. The vessel details are given in Table 1. The vessel is numerically simulated for different speeds. The results of the present numerical study and experimental data are reported in Fig. 10.

Figure 10 and Table 6 shows the comparison of CFD results with the experimental ones for resistance and trim without interceptor for a range of beam Froude numbers of 1.56–2.28. It is observed that the resistance of the vessel obtained from experiments for the hull without interceptor is in good agreement with the CFD results. The total resistance increases with speed, whereas the trim increases marginally and then decreases. With the increase in speed, the resistance increases and trim reduces. The trend is the same in both numerical and experimental study. Literature reports slight over-prediction of resistance by CFD simulation when compared with experimental results for bare hull (Banks et al. 2016). Therefore it is perhaps due to the inaccuracy in representing the flow physics around the vessel at the planing speed, consequent to the limitations of the RANSE solver parameter settings and numerical approximations and assumptions in the CFD analysis.

The comparison of CFD results with experimental ones for resistance and trim with interceptor (1 mm) for various beam Froude numbers are shown in Fig. 11 and Table 7. It is observed that the vessel trim reduces with speed, substantiated by both CFD and experimental results with good correspondence. The vessel resistance results also show good correspondence and the same trend of increase with vessel speed.

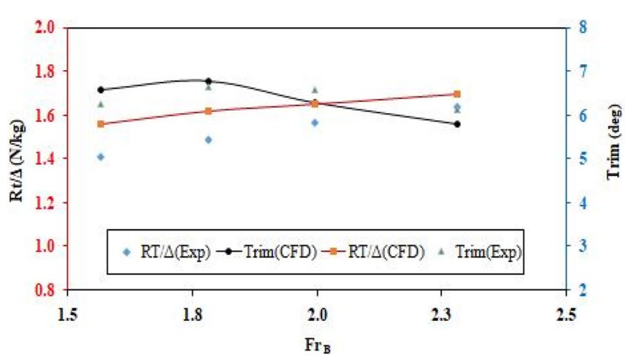

Fig. 10 Comparison of resistance and trim (experimental and CFD) results for the bare hull at different beam Froude numbers

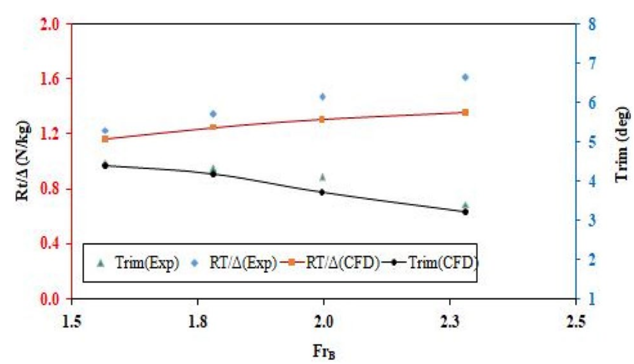

Fig. 11 Comparison of resistance and trim (experimental and CFD) results for the hull with interceptor (1 mm) at different beam Froude numbers

Table 6 Comparison of experimental and present computational trim (by stern) for bare hull at different Froude numbers

Fr_B	R_t/Δ (N/kg) Barehull (Exp)	R_t/Δ (N/kg) Barehull (CFD)	% error	Trim (°) Barehull (Exp)	Trim (°) Barehull (CFD)	% error
1.57	1.41	1.56	9.6	6.26	6.6	5.28
1.78	1.49	1.62	6.4	6.65	6.8	2.23
2.0	1.57	1.65	4.9	6.58	6.3	4.34
2.28	1.64	1.70	3.6	6.13	5.8	5.38

Table 7 Comparison of experimental and present computational trim (by stern) for hull with interceptor at different Froude numbers

Fr_B	R_t/Δ (N/kg) (Int) Exp	R_t/Δ (N/kg) (Int) CFD	% error	Trim (°) (Int) Exp	Trim (°) (Int) CFD	% error
1.57	1.23	1.16	5.8	4.48	4.38	2.25
1.78	1.35	1.25	7.6	4.32	4.19	3.05
2.0	1.47	1.31	8.5	4.10	3.70	8.92
2.28	1.61	1.46	9.2	3.41	3.20	6.06

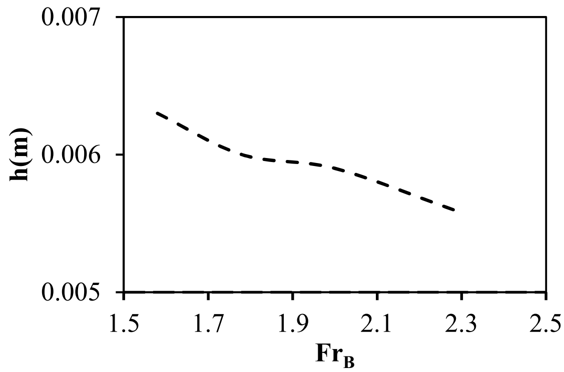

Fig. 12 Boundary layer thickness at transom for different Froude numbers

From Fig. 12 it is observed that the boundary layer thickness (h) is decreasing at the transom with increase in beam Froude number. As mentioned earlier the beam Froude number is given by $Fr_B = V/\sqrt{gB}$. The thickness of turbulent boundary layer can be calculated by the equation $h = 0.382 \times L_{WL}/(Re)^{0.2}$ (Schlichting 1979), where L_{WL} is the length of the water line, Re is the Reynolds number.

6.3 Numerical study for model fitted with flap

The numerical simulations are carried out on the model fitted with flap with different angular orientations for various speeds to study their hydrodynamic effects on the vessel performance.

The CFD results for resistance and trim of the model fitted with flap at different beam Froude numbers, are presented in Fig. 13. Figure 13 shows the resistance and trim for 0°, 4° and 8° flap. Stern flaps of 0°, 4° and 8° are used to study the resistance and trim effects on the craft. We considered the chord length with 2.5% of vessel length but with a different degree of flap angle. For the initial speeds, the 0° flap is showing a reduction in resistance when compared to 4° and 8° flap. As shown in Fig. 13 we observe that with increase in speed the resistance is increasing and the trim of the vessel is decreasing. When compared individually the interceptor is performing well than flap for the considered vessel.

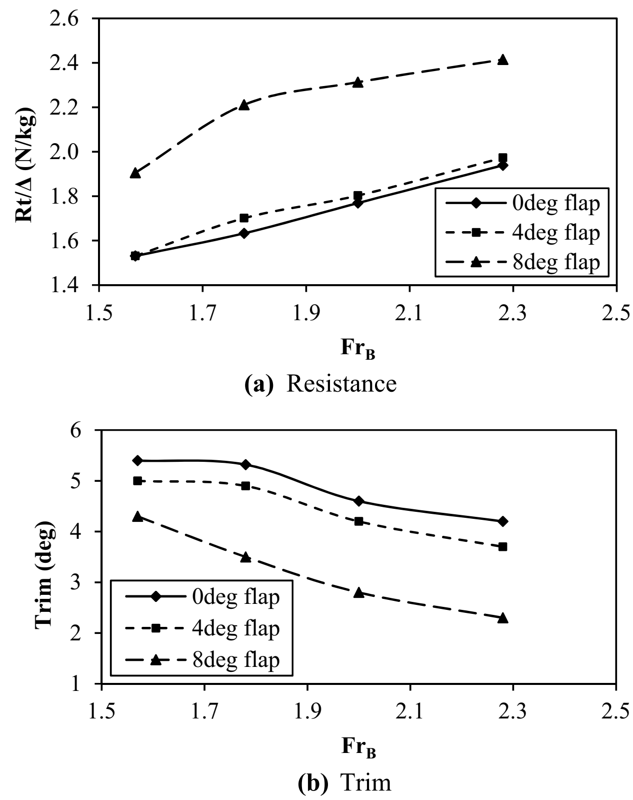

Fig. 13 CFD results for the hull resistance and trim for flap with different angular orientations

6.4 Numerical study for model fitted with Interceptor and stern flap combination

The numerical simulations are carried out on the model fitted with a combination of stern interceptor and flap with different angular orientations for various speeds to study their combined hydrodynamic effects on the vessel performance.

The CFD results for resistance and trim of the model fitted with both interceptor and flap, with the model operated at different beam Froude numbers, are presented in Fig. 14. Figure 14a shows the resistance of the hull without interceptor and flap and those with a combination of interceptor and flap, with the flap at different angular orientations. It shows that the resistance of the hull without interceptor-flap is more compared to the hull with interceptor-flap. It is

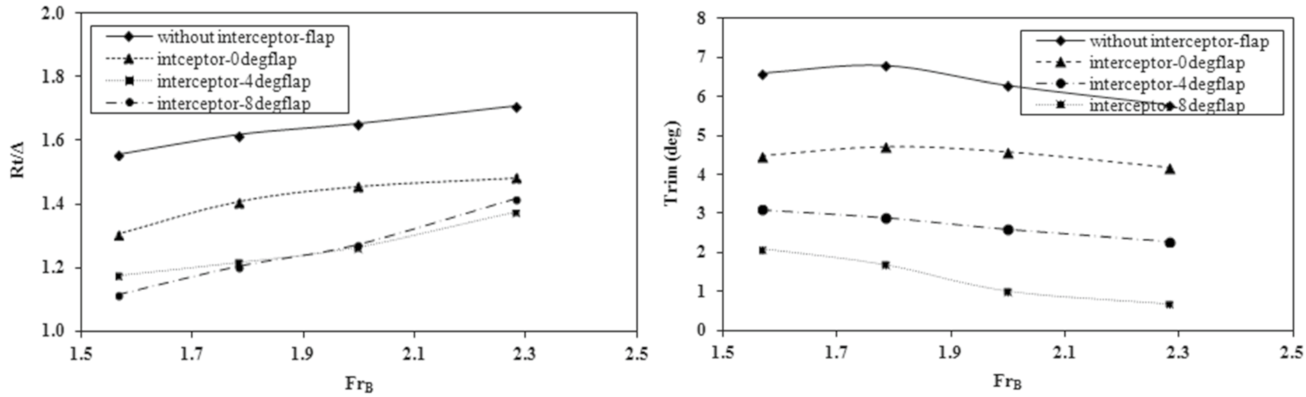

(a) Resistance (b) Trim

Fig. 14 CFD results for the hull resistance and trim with interceptor and flap of different orientations

Table 8 Comparison of resistance for interceptor with different flap angular orientations

Fr_B	R_t/Δ (N/kg) (Interceptor-0° flap)	R_t/Δ (N/kg) (Interceptor-4° flap)	R_t/Δ (N/kg) (Interceptor-8° flap)
1.57	1.31	1.18	1.12
1.78	1.41	1.22	1.20
2.0	1.46	1.27	1.27
2.28	1.48	1.37	1.41

Table 9 Comparison of trim (by stern) for interceptor with different flap angular orientations

Fr_B	Trim (°) (interceptor-0° flap)	Trim (°) (interceptor-4° flap)	Trim (°) (interceptor-8° flap)
1.57	4.5	3.1	2.1
1.78	4.7	2.9	1.7
2.00	4.6	2.6	1.03
2.28	4.2	2.3	0.7

noted that for different orientations of the flap attached to the interceptor, there is a decrease in resistance. With the increase in model speed, the resistance also increases. It has been observed that the case with a flap angle 4° gives better performance, particularly at design speed, where the resistance is less compared to other cases of flap angular orientations. Figure 14b displays the trim comparison of CFD results for the hull without interceptor-flap and with interceptor-flap of different angles. With the increase in speed, the trim is decreasing. It is noted that for different orientations of the flap attached to the interceptor, there is a decrease in trim angle for different Froude numbers. Higher pressure with increased flap angle resulted in reduced trim. The increase in the waterline length leads to reduced Froude number for the hull with interceptor flap at 4° and hence it reduces the wave-making resistance compared to the hull with interceptor flap at 8°, at 2.29 beam Froude number.

Resistance and trim for interceptor attached with different angular orientations are shown in Tables 8 and 9. The trim of the vessel is taken by stern for different Froude numbers. Out of the three flap angular orientations 4° showed better performance at the design speed.

Comparison of CFD results for (a) resistance and (b) trim at different beam Froude numbers for the hull without interceptor, with 1 mm interceptor and interceptor-flap with 4° are shown in Fig. 15. The resistance of the hull with interceptor-flap at 4° is less compared to the case without interceptor and also the case with 1 mm interceptor. This decrease in resistance on the hull for the case with interceptor-flap combination is due to reduced trim and also due to the increased wetted length. There is a reduction of 19–24% in resistance (Table 10) and trim reduction of 53–60% (Table 11) for the case with interceptor-flap at 4° in the range of speeds considered here when compared to the hull without interceptor-flap.

There is a reduction of 1–4% in resistance and trim reduction of 20–30% (Table 12) for the case with interceptor-flap at 4° in the range of speeds considered here, when compared to the hull with 1 mm interceptor. It is also noted that there is a reduction in vessel trim with increase in speed. Thus, from the present study, it is evident that the use of interceptor-flap reduces the vessel resistance and also its trim.

Resistance and trim for the bare hull, 1 mm interceptor and interceptor-flap with 4° at $Fr_B = 1.78$ with their percentage reduction is shown in Fig. 16. It is perceived that there is good percentage reduction in vessel trim when 4°

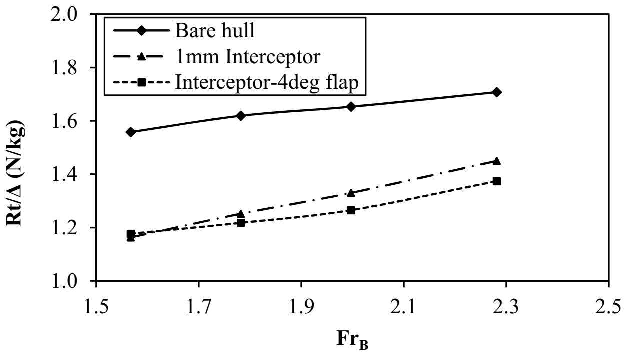

(a) Resistance

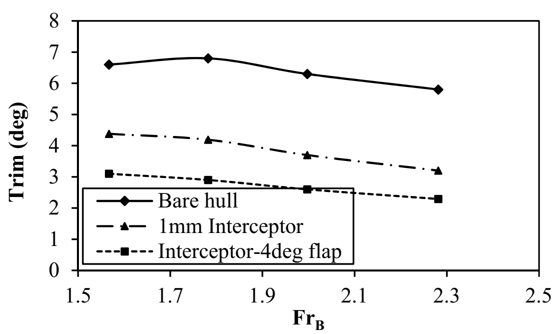

(b) Trim

Fig. 15 Comparison for hull resistance and trim (by stern) without interceptor, with 1 mm interceptor and interceptor-flap with 4° at different Froude numbers

Table 10 Percentage reduction in resistance in comparison with bare hull, 1 mm interceptor and interceptor 4° flap

Fr_B	R_t/Δ (N/kg) (CFD)	R_t (% reduction) 1 mm Interceptor	R_t (% reduction) Interceptor-flap
1.57	1.56	25.32	24.45
1.78	1.62	22.68	24.78
2.0	1.65	20.57	23.45
2.28	1.70	20.32	19.52

Table 11 Percentage reduction in trim (by stern) in comparison with bare hull, 1 mm interceptor and interceptor 4° flap

Fr_B	Trim (Bare hull)	Trim (% reduction) 1 mm Interceptor	Trim (% reduction) Interceptor-flap
1.57	6.26	33.63	53.03
1.78	6.65	38.38	57.35
2.0	6.58	41.26	58.73
2.28	6.13	44.82	60.51

Table 12 Percentage reduction in resistance and trim (by stern) in comparison with 1 mm interceptor and interceptor 4° flap

Fr_B	R_t (% reduction between) 1 mm interceptor—interceptor-flap	Trim (% reduction between) 1 mm interceptor—interceptor-flap
1.57	1.16	29.22
1.78	2.71	30.78
2.0	3.62	20.00
2.28	1.0	28.43

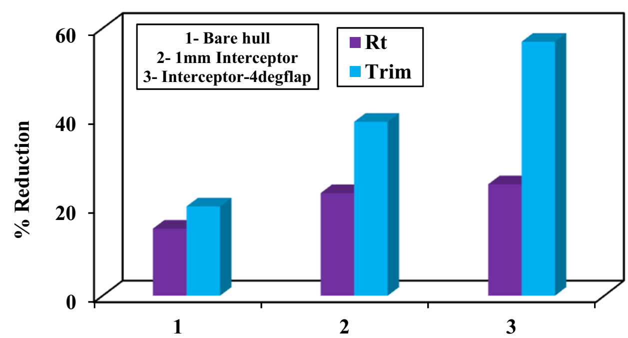

Fig. 16 Comparison of resistance and trim for the for bare hull, 1 mm interceptor and interceptor-4° flap at $Fr_B = 1.78$ with base case as bare hull

flap is attached to 1 mm interceptor. There is also reduction in resistance when compared with bare hull and 1 mm interceptor.

6.5 Effect on vessel sinkage

A ship advancing through water undergoes sinkage and trim due to hydrodynamic forces acting on ship hull.

Figure 17 presents sinkage of the hull with and without interceptor and interceptor with flap at 4°. The sinkage of the hull shows a good benefit on the hull considered here with interceptor-flap. Among the three cases (A, B, C in Table 13), it is clearly understood that case C, (that is, the vessel with interceptor-flap combination at stern) is more effective, where sinkage, trim and resistance are less compared to cases A and B. The variable S_W is representing the wetted surface in the present study. Considering the forces acting on the fully planing vessel the running trim angle exceeds 4°–5°. Therefore, in the bare hull case it can be assumed that the transom can be unwetted (Carlton 2019). Whereas, the hull fitted with interceptor experiences a reduction in the trim of the vessel as it increases the pressure beneath the hull surface. At high Froude numbers, there is a flow separation at

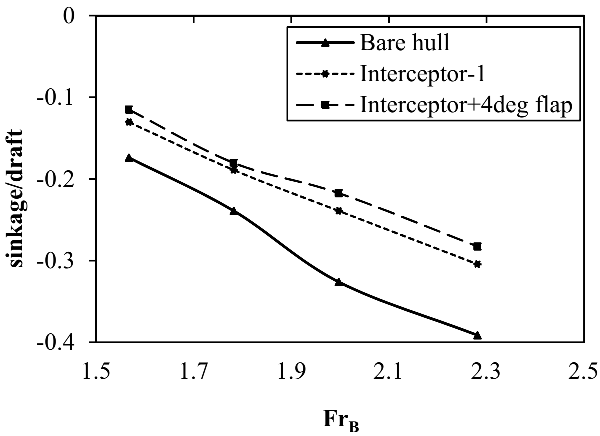

(a) Sinkage

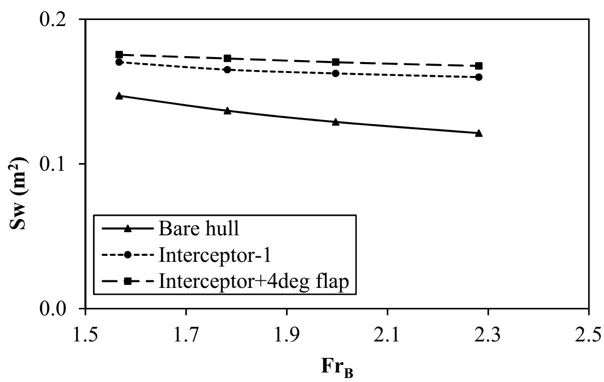

(b) Wetted surface

Fig. 17 **a** Plot of sinkage at CG, **b** plot of wetted surface (S_W) of the hull for cases with and without interceptor and with interceptor-flap (4°) combination

the interceptor which forms a hollow behind the transom of the vessel resulting in a small proportion of wetted transom.

Sinkage for the bare hull, 1 mm interceptor and interceptor with flap at 4° are presented in Fig. 18a at $Fr_B = 1.78$. The percentage reduction of sinkage for the hull with 1 mm interceptor and interceptor with flap at 4° in comparison with the bare hull is shown in Fig. 18b at $Fr_B = 1.78$.

6.6 Pressure distribution

The pressure distribution on the bottom of the hull for the cases without interceptor and with 1 mm interceptor and then with the integrated interceptor-flap, with 4° angular orientation, are shown in Fig. 19.

It is observed that the pressure at transom for the hull without interceptor is less compared to the other two cases. When the hull is fitted with interceptor, the pressure increased at the transom and the vessel trim reduced. For the case where the transom is fitted with an integrated interceptor-flap, the pressure increased (Fig. 20) further resulting in a more favorable reduction of the vessel trim.

7 Summary and conclusion

A planing hull vessel is investigated both experimentally and numerically to assess its hydrodynamic performance when it is fitted with interceptor and integrated interceptor-flap system at the vessel transom. Experimental tests were performed in the Towing Tank facility at IIT Madras in calm water condition for the cases of the hull with and without interceptor. Numerical studies are carried out for the same vessel and for the above-mentioned cases using RANSE solver (Star CCM+). The numerical results of resistance and trim values are compared with experimental results and good correspondence is noticed. Subsequently, the numerical study is extended for the hull fitted with integrated interceptor-flap with the flap at different angular orientations and its effect of resistance, trim and sinkage on the vessel is noted.

The conclusions drawn from this study are:

- The interceptor decreases the drag of the hull by 5–15% at different speeds varying from $Fr_B = 1.0–2.28$ when compared to the bare hull. This reduction in resistance is due to the lift caused due to pressure creation on the vessel by the interceptor at the transom.
- Trim is reduced by 32–45% at different speeds which shows that the interceptor mainly acts as a trim control device.
- The integrated interceptor-flap fixture, with flap at 4°, the drag of the hull decreased by 19–24% for $Fr_B = 1.0–$

Table 13 Effect of resistance, trim and sinkage for the hull with and without interceptor and with interceptor-4° flap

FnB	Rt/Δ			Trim (°)			Sinkage (at LCG)			Wetted surface (m^2)		
	A	*B*	*C*	*A*	*B*	*C*	*A*	*B*	*C*	*A*	*B*	*C*
1.78	1.62	1.25	1.22	6.8	4.2	2.9	−0.24	−0.19	−0.18	0.14	0.165	0.173
2.0	1.65	1.31	1.27	6.3	3.7	2.6	−0.33	−0.24	−0.22	0.13	0.162	0.170
2.28	1.70	1.36	1.37	5.8	3.2	2.3	−0.39	−0.31	−0.28	0.12	0.159	0.167

A—without intercept and flap, *B*—with 1 mm interceptor, *C*—with 1 mm interceptor-4° flap

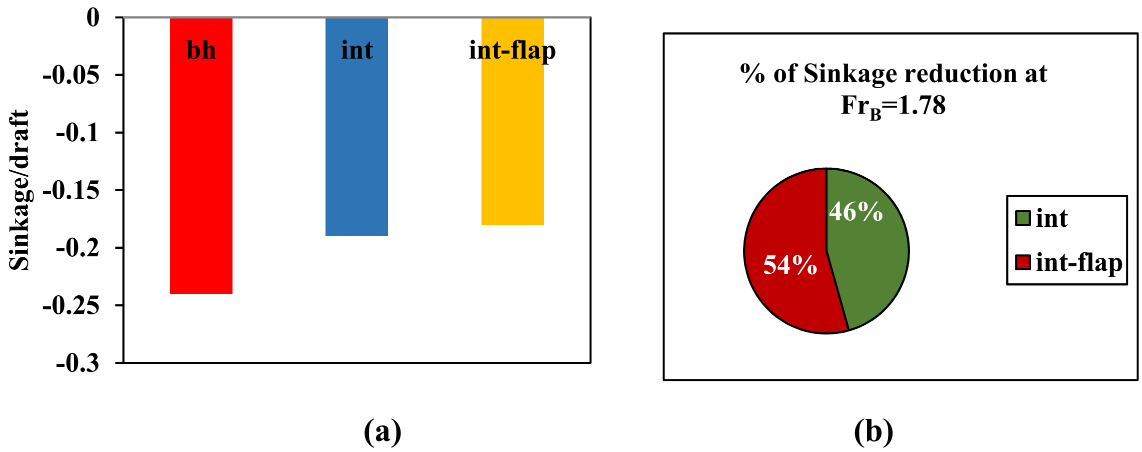

Fig. 18 **a** Displays sinkage of the bare hull, 1 mm interceptor and interceptor with flap at 4° and **b** % reduction of sinkage for 1 mm interceptor and interceptor with flap at 4° at $Fr_B = 1.78$

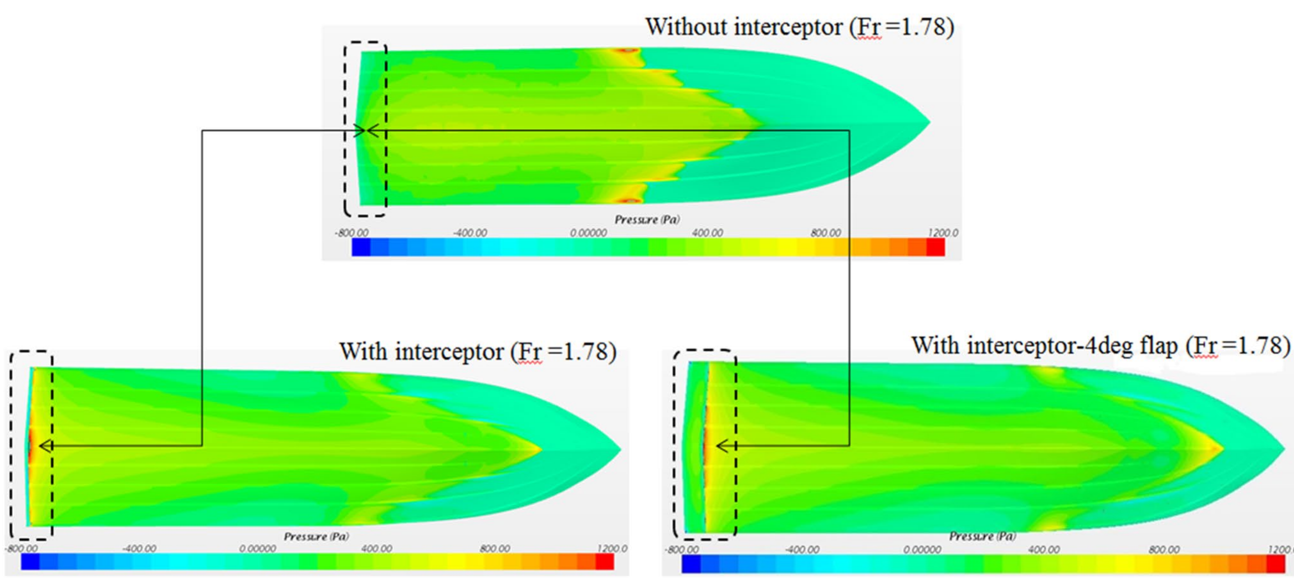

Fig. 19 Pressure contour on the hull bottom for the hull with and without interceptor and interceptor-flap (4°) at $Fr_B = 1.78$

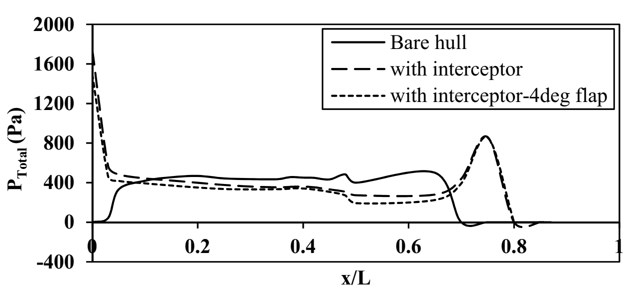

Fig. 20 Total pressure distribution on the bottom of the hull at centreline

2.28 when compared to the bare hull. This reduction in resistance is due to the further reduction in wave-making resistance.

- The pressure created by the interceptor and the integrated interceptor-flap at the hull transom helps in the reduction of trim on the vessel.
- Integrated interceptor-flap showed a reduction of trim by 53–60% when compared to the bare hull at different speeds which shows that it also acts as a trim control device.

- The hull with interceptor and integrated interceptor-flap show a positive effect on the sinkage of the vessel when compared to the bare hull. The vessel sinkage is less in B and C cases due to the higher pressure created by the fixtures at the stern.
- It is observed that the hull with 1 mm interceptor performs better than 2 mm interceptor which implies that the right height of the interceptor is important for the performance of the vessel. The integrated interceptor-flap, with 4° flap, is more effective from the hydrodynamic aspects compared to the other two cases, with and without interceptor.

Appendix A

Grid, iterative and time-step convergence verification study

The response variables, which are analysed in the simulations are the total resistance coefficient (C_T), pressure resistance coefficient (C_F), wetted surface area (S_W) and running trim (τ). The resistance coefficients are evaluated using the formula:

$$C_T = R_T/0.5\rho S_W V^2, \tag{8}$$

$$C_F = R_F/0.5\rho S_W V^2. \tag{9}$$

The response variable S_W representing the wetted surface is estimated using the distribution of volume fraction of water (α) over the hull surface. The statistical convergence is estimated by calculating the difference of the mean obtained from the time history of the response variable in the asymptotic window with the mean in the last oscillation. The running mean of oscillations is less than 0.85% of the mean value for all response variables across the cases.

The grid convergence studies are performed using three progressively refined grids called Grid-A, B and C which are coarse, fine and finest, respectively, the cell count for each successive refinement increases approximately by a factor of $\sqrt{2}$; the details are given in Table 3.

The data obtained from grid dependency analysis is given in Table 14; the analysis uses the correction factor method from prescribed by Stern et al. (2001). It is established that the condition for monotonic convergence is achieved since for all the response variables considered, the grid convergence ratio (R_G) is less than one. The grid uncertainty parameter (U_G) shows the grid uncertainty for various variables such as C_T, C_P, trim and S_W in percentage. C_G denotes correction factor and P_G is the order of accuracy for various response variables. The statistical convergence is estimated by calculating the difference of the mean obtained from the time history of the response variable in the asymptotic window with the mean in the last oscillation. The running mean of oscillations is less than 0.8% of the mean value for all response variables across the cases.

Inner iterations are performed for convergence of solution in each time step and the iterative uncertainty is defined based on Stern et al. (2001). Table 15 shows the iterative uncertainty for all the response variables using Grid B at a speed of 25 knots. This study executes the simulations with ten inner iterations.

To obtain the time step uncertainty this study generates three solutions using the ratio of $\sqrt{2}$ between succeeding time steps. Table 16 shows the time step convergence analysis. The study performs simulations using corresponding Grid B which show that the convergence ratio (R_G) is less than unity, indicative of monotonic convergence towards the time step. The time step uncertainty for C_T and C_P is less than 0.6% for the mesh.

Validation

The validation of simulations follows the method based on Stern et al. (2001). It estimates the error between simulation results (S) and experimental data (D) namely, the comparison error (E) and the validation uncertainty (U_V) in it. Here uncertainty U_V is the combination of experimental uncertainties (U_D), simulation uncertainties (U_{SN}) and input uncertainty (U_{Input}). Simulation error and uncertainty have

Table 14 Grid dependency study for various response variables

	R_G	P_G	$\lvert 1 - C_G \rvert$	$(\%)U_G$
Total resistance coefficient (C_T)	0.86	0.88	0.79	8.74
Pressure resistance coefficient (C_P)	0.35	3.54	1.62	1.35
Running trim (τ)	0.85	0.64	0.85	3.47
Wetted surface area (S_W)	0.46	3.54	0.89	2.48

Table 15 Iterative convergence study for the Grid B at 25 knots speed (U_I values are a percentage of the solution with 10 inner iterations)

C_T U_I (%)	C_P U_I (%)	Trim U_I (%)	WSA U_I (%)
0.624	0.658	0.532	1.145

Table 16 Time step convergence analysis for a time step ratio $\sqrt{2}$ at a design speed of 25 knots (grid B)

	R_G	P_{TS}	$\lvert 1 - C_{TS} \rvert$	$(\%)U_{TS}$
Total resistance coefficient (C_T)	0.65	1.95	0.15	0.46
Pressure resistance coefficient (C_P)	0.17	6.24	4.94	0.53
Running trim (τ)	0.19	6.24	4.51	0.04
Wetted surface area (S_W)	0.18	5.21	4.25	0.31

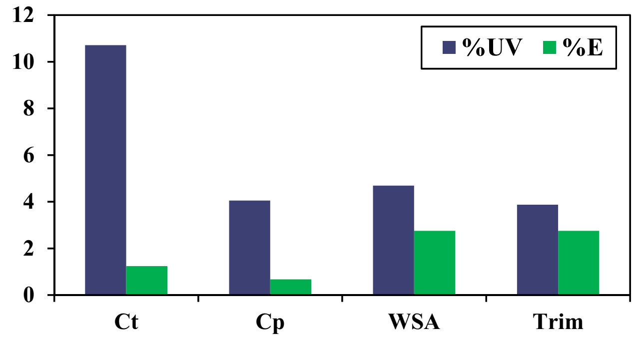

Fig. 21 Comparison between validation uncertainity and error

components from modelling, numerical and input elements. The modelling error is due to assumptions and approximations of the simulation model in representing the physical phenomena. The numerical error is introduced due to numerical computations based on the governing equations and the input error is due to the errors in the simulation input parameters.

$$E = D - S = \delta_D - (\delta_{SM} + \delta_{SN} + \delta_{input}), \tag{10}$$

$$U_V^2 = U_{SN}^2 + U_D^2 + U_{input}^2. \tag{11}$$

The uncertainty in the input data is related to the body geometry, and fluid parameters such as density and viscosity. It is assumed that the input uncertainty is negligible in comparison to other numerical uncertainties.

If $|E| < U_V$ i.e., the error lies within the validation uncertainty, then validation is achieved for this uncertainty level.

If $|E| > U_V$ i.e., the error lies outside the validation uncertainty, then validation has not been achieved for this uncertainty level and therefore, there is a need for improving the simulation modelling.

Figure 21 displays the validation uncertainty and error comparison. It shows that $|E| < U_V$ i.e., the error lies within the validation uncertainty, then the validation is achieved for this uncertainty level.

References

Anantha Subramanian V, Subramanyam PVV, Sulficker Ali N (2007) Pressure and drag influences due to tunnels in high speed planing craft. Int Shipbuild Prog 54:25–44

Avci AG, Barlas B (2018) An experimental investigation of interceptors for a high speed hull. Int J Naval Archit Ocean Eng 11:256–273

Brizzolara S (2003) Hydrodynamic analysis of interceptors with CFD methods. In: Proc. seventh international conference on fast sea transportation (FAST), vol 3

Carlton JS (2019) Resistance and Propulsion (Fourth edition)

Day AH, Cooper C (2011) An experimental study of interceptors for drag reduction on high-performance sailing yachts. Ocean Eng 38:983–994

De Luca F, Pensa C (2011) Experimental data on interceptor effectiveness. In: IX high speed marine vehicles, Naples

De Luca F, Mancini S, Miranda S, Pensa C (2016) An extended verification and validation study of CFD simulations for planing hulls. J Ship Res 60(2):101–118

Deng R, Debo H, Zhou G, Sun H (2011). Preliminary numerical investigation of effect of interceptor on ship resistance

Faltinsen O (2005) Hydrodynamics of high speed marine vehicles, Chap. 10. Cambridge University Press, Cambridge

Ghassemi H, Mansouri M, Zaferanlouei S (2011) Interceptor hydrodynamic analysis for handling trim control problems in the high speed crafts. Proc IMechE 225:2597–2618. https://doi.org/10.1177/0954406211406650.PartC:J.MechEngineeringScience

Hoekstra M (1999) Numerical simulation of ship stern flows with a space-marching Navier–Stokes method. Ph.D. thesis, Technical University of Delft, Delft, The Netherlands

Hung CB, Kim JJ (2007) Numerical study on the improvement of resistance performance for fast Ferry with transom appendage. J Mech Sci Technol 21:106–112

Insen M (1999) "Numerical Simulation of Ship Stern Flows With a Space-Marching Navier–Stokes Method," Ph.D. thesis, University of Southampton, Southampton, UK

ITTC (2002) Model manufacturing ship models. In: 23rd international towing tank conference, (7.5-02-05-01), pp 1–6, Revision-01

ITTC (2011) Practical guidelines for ship CFD applications, (7.5-03-02-03), pp 1–18, Revision-01

Jangam S, Krishnankutty P, Anantha Subramanian V (2018) Numerical study on Hydrodynamic performance of integrated interceptor-flap fitted to the transom of planing vessel. In: 37th international conference on ocean offshore and arctic engineering (OMAE), Madrid, Spain, June 17–22

John S, Kareem Khan MD, Praveen PC, Manu K, Panigrahi PK (2011) Hydrodynamic performance enhancement using stern wedges, stern flaps and interceptors. In: ICSOT

Karafiath G, Cusanelli DS, Lin CW (1999) Stern wedges and stern flaps for improved powering—US navy experience. In: SNAME annual meeting, Baltimore

Karimi HM, Seif SM, Abbaspoor M (2013) An experimental study of interceptors effectiveness on hydrodynamic performance of high-speed planing crafts. Polish Marit Res 2(78)20:21-29

Li PY, Qiu YM, Gu MT (2002) Study of trimaran wave making resistance with numerical calculation and experiments. J Hydrodyn 14(2):99–105

Mansoori M, Fernandes AC (2015) Hydrodynamics of the interceptor on a 2-D flat plate by CFD and experiments. J Hydrodyn 27(6):919–933

Mansoori M, Fernandes AC (2017a) Hydrodynamics of the Interceptor Analysis via both Ultra reduced model test and dynamic computational fluid dynamics simulation. J Offshore Mecha Arctic Eng 139:021101-1

Mansoori M, Fernandes AC, Ghassemi H (2017b) Interceptor design for optimum trim control and minimum resistance of planing boats. J Appl Ocean Res. https://doi.org/10.1016/j.apor.2017.10.006

Mansoori M, Fernandes AC, Ghassemi H (2017) Interceptor design for optimum trim control and minimum resistance of planing boats. J Appl Ocean Res. https://doi.org/10.1016/j.apor.2017.10.006

Marin JR, Benites DA (2012) Side-boat tow to TEST the influence of flaps in a 2-meter planing craft model. Ship Sci Technol 6(11):67–78

Millward A (1976) Effect of wedges on the performance characteristics of two planing hulls. J Ship Res 20(4):224–232

Molini A, Brizzolara S (2005) Hydrodynamics of Interceptors: a fundamental study. In: International conference on maritime research and transportation, ICMRT, vol 1, Ischia, Italy

Raven HC, van Brummelen EH (1999) A new approach to computing steady free-surface viscous flow problems. In: 1st MARNET-CFD workshop, Barcelona, Spain, p 4

Salas M, Tampier G (2013) Assessment of appendage effect on forwarding resistance reduction. Ship Sci Technol 7(13):37–45 (**Cartagena (Columbia)**)

Savitsky D (1964) Hydrodynamic Design of Planning Hull. Marine Technol 8(4)

Schlichting H (1979) Boundary layer theory, 7th edn. McGraw-Hill Inc., New York

Song K, Guo C, Wang C, Gong J, Li P (2018) Influence of interceptors, stern flaps and their combination on the hydrodynamic performance of deep V ship. Ocean Eng 170:306–320

Srikanth Syamsundar S, Datla R (2008) Performance prediction of high-speed planing craft with interceptors using a variation of the Savitsky method. In: The First Chesapeake Power Boat Symposium, Annapolis, Maryland, USA

Stern F, Wilson R, Coleman H, Paterson E (1997) Comprehensive approach to verification and validation of CFD simulation Part 1: Methodology and Procedures. J Fluids Eng 123(4):793–802

Stern F, Wilson R, Coleman H, Paterson E (2001) Comprehensive approach to verification and validation of CFD simulation. Part 1: methodology and procedures. J Fluids Eng 123(4):793–802

Suneela J, Krishnankutty P, Anantha Subramanian V (2020) Numerical investigation on the hydrodynamic performance of high-speed planing hull with transom interceptor. J Ships Offshore Struct 15(11):1–9

Suneela J, Krishnankutty P, Anantha Subramanian V (2018) Numerical study on Hydrodynamic performance of integrated interceptor-flap fitted to the transom of planing vessel. In: 37th International conference on Ocean Offshore and Arctic Engineering (OMAE), Madrid, Spain, June 17-22

Tsai J, Hwang J, Chou S (2004) Study on the compound effects of interceptor with stern flap for two fast monohulls. OCEANS ’04. MTTS/IEEE TECHNO-OCEAN ’04 vol 2. https://doi.org/10.1109/OCEANS.2004.1405650

Villa D, Brizzolara S (2009) A systematic CFD analysis of flaps / interceptors hydrodynamic performance. In: Proceedings of 10th international conference of fast sea transportation, Athens, Greece

Visone M, Bertetti P, Gandolfi R, Falletta C, Ausonio PL, Paterna D et al (2005) VOF-dynamic mesh simulations of unsteady ship hydrodynamics. In: Marine CFD—4th international conference on marine hydrodynamics. The Royal Institution of Naval Architects, London